Soft Matter

Self-Assembled Materials from Cellulose Nanocrystals Conjugated with a Thermotropic Liquid Crystalline Moiety

Journal:	*Soft Matter*
Manuscript ID	SM-ART-07-2022-000906.R2
Article Type:	Paper
Date Submitted by the Author:	28-Sep-2022
Complete List of Authors:	Masese, Francis; University of Connecticut, Chemistry Ndaya, Dennis; University of Connecticut, Storrs, Department of Chemistry and Polymer Program, IMS Liu, Chung-Hao; University of Connecticut, Polymer Program, Institute of Materials Science Eddy, Nicholas; University of Connecticut, Chemistry Morales-Acosta, Daniela; University of Connecticut, Storrs, Institute of Materials Science Nieh, Mu-Ping; University of Connecticut, Chemical and Biomolecular Engineering; University of Connecticut, Polymer Program, Institute of Materials Science Kasi, Rajeswari; University of Connecticut, Storrs, Chemistry and Polymer Program, IMS

Self-Assembled Materials from Cellulose Nanocrystals Conjugated with a Thermotropic Liquid Crystalline Moiety

Francis K. Masese[†], Dennis Ndaya[†§], Chung-Hao Liu[§], Nicholas Eddy[†§], M. Daniela Morales-Acosta[§], Mu-Ping Nieh[§δ], Rajeswari M. Kasi[†§]

[†]Department of Chemistry, University of Connecticut, Storrs, CT 06269 (USA)

[§]Polymer Program, Institute of Material Science, University of Connecticut, Storrs, CT 06269

[δ]Department of Chemical & Biomolecular Engineering, University of Connecticut, Storrs, CT 06269

[*]Authors to whom correspondence should be addressed.

Prof. R M Kasi: rajeswari.kasi@uconn.edu; Tel: +1 (860)-486-4713

Abstract

Manipulating molecular and supramolecular interactions within cellulose nanocrystals (CNCs) to introduce different levels of assemblies combined with multiple functionalities is required for the development of degradable smart materials from renewable resources. To attain hierarchical structures and stimuli-responsive properties, a new class of liquid crystalline cellulosic hybrid materials is synthesized. Herein, main-chain rigid-rod like oxidized cellulose (CNC-COOH) is prepared from Cellulose Whatman filter paper (Cellulose W.P.) by acid hydrolysis and oxidized using the 2,2,6,6-tetramethyl-1-piperidinyloxy (TEMPO). Thermotropic LC molecule, 4-cyano-4'-hydroxybiphenyl with a 12-methylene spacer (CB12-OH), is grafted onto the carboxylic acid group of CNC-COOH via Steglich esterification. The liquid crystalline functionalized CNCs cellulose nanocrystals (CNC-COO-CB12) are readily soluble in DMSO and ionic liquids. The extent of functionalization and structure of CNC-COO-CB12 are confirmed by solution-state ^{1}H NMR and supported by other characterization techniques. We investigate the interplay of liquid crystalline orientational order of CNCs and cyanobiphenyl (CB12), and the supramolecular hydrogen bonding of CNCs within CNC-COO-CB12 and compare it with CNC-COOH. The introduction of thermotropic CB12 side chains onto rigid-rod CNCs shows the exclusive formation of smectic mesophases from the assemblies of CB12 with the absence of cholesteric mesophase typically observed from CNC-COOH as verified by temperature-controlled SAXS (T-SAXS). This is further verified by UV-visible and SEM studies that show CNC-COO-CB12 forms smectic domains while CNC-COOH forms visible light reflecting cholesteric mesophase in dried films. Thus, the interplay of liquid crystalline order of CNCs and CB12 and supramolecular hydrogen bonding of CNCs results in ordered, smectic-mesostructured CNCs for use in stimuli-responsive functional materials.

Keywords: Cellulose nanocrystals; TEMPO-oxidized cellulose nanocrystals; self-assembly, Stimuli-responsiveness; cyano biphenyl; 1-Butyl-3-methylimidazolium Acetate; dissolution; Main-chain/side-chain liquid-crystalline polymer; Smectic mesophase.

Introduction

Cellulose nanocrystals (CNCs) are rod-like, charged, semicrystalline materials with dimensions ranging from 5 to 20 nm in width and 100 to 500 nm in length and prepared through either the acidic or alkaline hydrolysis of cellulose biopolymer.[1-3] These rigid nanorod crystals are composed of chiral β(1⇒4) D-glucose subunits, which render CNCs structurally chiral with a twist in their internal structure and outer morphology.[4] These nanomaterials have been widely utilized to produce functional, environmentally friendly, sustainable composites and nanocomposites that are degradable.[5-7] The CNC size and surface chemistry highly depend on the hydrolysis conditions and the cellulose source. Aqueous suspension of sulfonated or carboxylated CNCs exhibits lyotropic phase behavior transitioning from an isotropic to a biphasic suspension to an LC phase with increasing concentration.[8-10] Moreover, at higher weight percent concentration, these suspensions transition to a birefringent gel-like material, in which CNCs self-assemble into cholesteric or chiral nematic (Ch*) liquid crystals (LC)s [5, 11, 12] The optical properties of cholesteric LCs are controlled by the pitch of the helix, which is impacted by dispersion composition, ionic strength of the medium, particle size, and temperature.[13]

Molecular liquid crystals (LCs) or liquid crystalline polymers (LCPs) have been grafted onto CNCs to enhance dispersion and solubility in different solvents and to manipulate self-assembly in lyotropic gels and dried films. Surface modification of cellulose nanocrystals with different nematic liquid crystals has been used to modulate chirality transfer from an innately chiral

nanocrystal core at both the molecular and the macroscopic levels.[4] For example, achiral LC molecules such as 6-[(4'-cyano-4-yl)oxy]-hexanoic acid or 6-[[4'-(heptyloxy)-[1,1'-biphenyl]-4-yl]oxy]-hexanoic acid are tagged on the chiral CNCs surface by chemical conjugation. After sonication, these guest LC molecules only marginally enhance the efficacy of helical distortion of the host CNC matrix. This indicates a high propensity for the non-chiral LC molecule to become a part of cholesteric LC mesophase and their resultant properties in lyotropic gels and dried films.[4] When a cyanobiphenyl molecule with 6 methylene spacer is attached to CNC, the cyanobiphenyl gets incorporated into the self-assembled cholesteric mesophase. Furthermore, when a chiral liquid crystalline molecule such as cholesterol is covalently bonded to CNC's chiral core as well as the surface, the efficacy of helical distortion of the CNC is also marginally enhanced from lyotropic suspensions.[4] These results show that the substitution of the hydrophilic environment of CNC with a more hydrophobic nematic LC molecule permits CNCs to self-assemble into chiral nematic LC phase with a similar *p* at two orders of magnitude lower CNC concentration.[4, 14, 15]

In another approach, azo polymers are successfully grafted from CNC via atom transfer radical polymerization (ATRP) to produce an amphitropic polymer, which exhibits liquid-crystalline behavior both in lyotropic and thermotropic states.[16] Moreover, PMMAZO-grafted CNC maintains a smectic texture at room temperature and shows smectic-to-nematic transition at 95 °C and nematic-to-isotropic transition at 135 °C.[16] In chlorobenzene, this system shows a lyotropic nematic phase above a concentration of 5.1 wt%[16]. In another example, anionic polyelectrolyte, poly(sodium 4-styrene sulfonate) (PSS) was grafted from CNCs modified ATRP-initiator, resulting in CNCs grafted with PSS.[17] At 4 w% in 1 mM NaCl, the CNC grafted with PSS demonstrated no order. However, studies at 5 w% revealed nematic ordering.[17]

Ethyl cellulose (EC) has also been grafted on 3,4,5-tris[4-(dodecyloxy) benzyloxy] benzoate (EC-g-DOBOB) using dicyclohexylcarbodiimide (DCC) and (dimethylamine) pyridinium-4-toluenesulfonate (DPTS) as the catalyst. The ethyl cellulose (EC) is the backbone, and the mesogenic moiety DOBOB (3,4,5-tris(4-(dodecyloxy)benzyloxy) benzoic acid) dendron is the side chain molecule. The dissolution of the sample in concentrated chloroform revealed lyotropic cholesteric liquid crystal with a planar texture.[18] 4-(4-Methoxyazobenzene-4'-yloxy)butyric acid is grafted on ethyl cellulose in DCC and DMAP, resulting in the polymer AzoEC with ethyl cellulose as the primary chain crystalline polymer and the azo mesogenic unit as the side chain polymer.[19] This novel polymer with a low degree of substitution shows the cholesteric phase inherent with ethylcellulose.[19] However, an increased degree of substitution to 0.33 results in fascinating supramolecular structures that consist of a large-scale ordered lamellar structure constructed by EC main chains and relatively small-scale ordered structures formed by azobenzene moieties. The formation of these ordered structures is ascribed to the interactions between the rod-like ethyl cellulose main-chain and the side groups and the π–π stacking of azobenzene mesogens in different temperature regions.[19] However, the transition temperatures to access these mesophases are typically above 150 ºC, which makes processing these samples for applications difficult.

We noted from the work of Hegman[4] and Chang[20] that four [$(CH_2)_4$] to five methylene spacers [$(CH_2)_5$] used to attach thermotropic LCs to CNCs can be used to improve the solubility of CNCs in organic solvents. We question if longer spacers between CNCs and thermotropic LCs can be used to decouple the mobility of CNCs from the LCs, resulting in improved solubility, tunable clearing temperatures, improved processing conditions, and easy formation of non-nematic mesophases including smectics, columnar or discotic structures. Thus, we report the synthesis of

novel cellulosic liquid crystalline hybrid materials conjugated with thermotropic liquid crystalline molecule (cyanobiphenyl) through a 12-methylene spacer [$(CH_2)_{12}$] unit. We investigate the interplay of the orientational order of the main-chain liquid crystalline CNCs and the side-chain thermotropic liquid crystal of CB12 molecules. We hypothesize that if CB-CB interactions dominate, then CNC-COO-CB12 will self-assemble into smectic domains in dried films, but if CNC-CNC interactions dominate, then CNC-COO-CB12 will self-assemble into cholesteric domains in dried films. The molecular manipulation of cellulose nanocrystal scaffolds by chemically installing a liquid crystalline mesogen will serve to create the next generation of responsive, functional, sustainable, and degradable CNC-based liquid crystalline materials.

Experimental

Materials

12-bromo-1-dodecanol (95%) and 4-cyano-4-hydroxybiphenl are purchased from TCI America, 4-Dimethylaminopyridine (99.0%), dimethyl sulfoxide (99.0), 1-butyl-3-methylimidazolium acetate > 95%, and 1-ethyl-3-(3-dimethylaminopropyl)carbodiimide hydrochloride, EDC.HCl (98.0%), Sodium hydroxide (>97%), sodium hypochlorite solution, (reagent grade), lithium chloride (99%), N,N-dimethylacetamide (>99.8%), methanol (>99.8%), and TEMPO (2,2,6,6-tetramethyl-1-piperidinyloxy) (98%) are obtained from Sigma Aldrich, Grade 1 quality filter paper standard grade is obtained from Cytiva life Sciences, sulfuric acid (95-98%) is obtained from Acros Organics, Hydrochloric acid (36.5 to 38.0%) is obtained from Fisher Scientific, and Dialysis membrane 12-14kDa MWCO is obtained from Cole-Parmer.

Synthesis of cellulose nanocrystal from cellulose using acid hydrolysis

Briefly, 5.2 g of cellulose Whatman filter paper (W.P.) is blended with 250 mL of deionized water to form a pulp. Sulfuric acid (140 mL) is slowly added to this pulp under vigorous mechanical stirring (250 mL, 20 °C). The resulting suspension is held at 50°C and magnetically stirred at 200 rpm for 3.5 hours to allow hydrolysis. After hydrolysis, the mixture is cooled at room temperature and washed via centrifugation at 6500 rpm for 5 minutes. This process is repeated until the pH value of the solution is about 3-4. The solution is dialyzed against distilled water for four days using dialysis membranes (12kDa-14kDa) until a pH value of 7 is obtained. Then the dispersion is sonicated for approximately 6 hours. The resulting suspensions are stored at 4 °C or freeze-dried till further use. Freeze-drying, or some form of drying, must remove as much moisture as possible before compounding.

TEMPO-mediated oxidation of CNCs in alkaline

TEMPO-oxidized CNCs are synthesized following the literature procedure.[21] 648 mg (4 mmol of glucosyl units) of CNCs are suspended in water (50 mL) containing 10 mg of 2,2,6,6-tetramethyl-1-piperidinyloxy (TEMPO, 0.065mmol) and 200 mg of sodium bromide (1.9 mmol) at room temperature for 30 minutes. The TEMPO-mediated oxidation of the CNCs is initiated by slowly adding 4.90 mL of 13% NaClO (8.6 mmol) over 20 min at room temperature under gentle agitation. The reaction pH is monitored using a pH meter and maintained at 10 by incrementally adding 0.5 NaOH. When no more decrease in pH is observed, the reaction is considered complete. About 5 mL of methanol is added to react and quench with the additional oxidant. After adjusting the pH to 7 by adding 0.5 M HCl, the TEMPO-oxidized product is washed with deionized water by centrifugation and further purified by dialysis against D.I. water for two days. 550 mg of solid

is recovered after freeze-drying. FTIR measurements showed a carboxylic acid peak at 1650 cm^{-1}.

Synthesis of p-toluene sulfonyl cyanobiphenyl

The synthesis of CB12-OH has been reported in a previous publication.[22] A new molecule, p-toluene sulfonyl cyanobiphenyl, abbreviated as CB12-OTs, is synthesized following a newly developed protocol. In a typical synthesis, CB12-OH (13.40 g, 39.34 mmol), p-Toluenesulfonyl chloride (5.0 g, 26.23 mmol), and triethylamine (33.17 g, 327.83 mmol) are transferred to a round-bottomed flask along with a magnetic stir bar, followed by addition of 40 mL of THF, and sealed with a rubber septum. The reaction mixture is purged with nitrogen for 10 minutes and then stirred in an oil bath for 48 h at 50 °C. The reaction mixture is cooled down to room temperature and diluted with 100 mL of ethanol to dissolve. The crude product is purified by recrystallization using 50 mL of ethanol, resulting in a white residue.

Synthesis of CNC-OO-CB12

A mixture of ionic liquid, 1-butyl-3-methylimidazolium acetate (14.29 g, 72.06 mmol), and DMSO (17.80 g, 229.87 mmol) in the ratio of 2.5:1 is prepared. TEMPO-oxidized CNCs abbreviated as CNC-COOH (1 g, 5.68mmol) are transferred to a round-bottomed flask and a magnetic stir bar, followed by 30 ml of the mixture, and sealed with a rubber septum. The reaction mixture is purged with nitrogen for 10 min and then stirred in an oil bath for 30 minutes at 80 °C to facilitate the dissolution of CNC-COOH. The reaction mixture is cooled down to room temperature and EDC.HCl (1.09 g, 5.68 mmol) in 10mL of the IL + DMSO mixture is added. The mixture is allowed to run for 30 minutes before the dropwise addition of DMAP (0.104 g, 0.85mmol) in 10mL of the IL + DMSO mixture. The synthesized CB12-OTs (3.57 g, 7.1mmol) are then added,

and the reaction mixture was stirred in the oil bath for 48 hours at 50°C. The mixture is precipitated using 200 mL of cold methanol and then washed twice with dichloromethane to dissolve any unreacted CB12-OTs. The residue is dried in a vacuum oven for 12 hours at 60 °C.

Results and Discussion

The CNC-COOH is prepared from cellulose Whatman filter paper using 2,2,6,6-tetramethylpiperidine-1-oxyl radical (TEMPO)–mediated radical oxidation. This process involves the partial conversion of the C6 primary hydroxyl group of the β-> 1,4 linked d-glucose units to the C6 carboxylate group. The electrostatic charge resulting from the carboxylate anion on the surface of CNC-COOH serves to stabilize the nanocrystal colloidal dispersions against aggregation in water and other polar solvents. The synthesized CNC-COOH is further conjugated with a cyanobiphenyl liquid crystalline unit with 12 methylene spacers by Stiglich esterification (Figure 1).

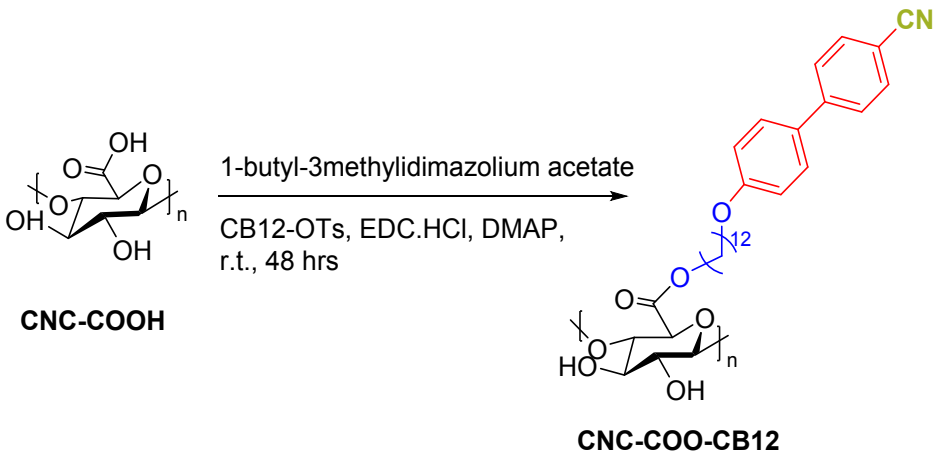

Figure 1. Synthesis of CNC-COO-CB12

Dissolution of Cellulose Nanocrystals

The cellulose W.P. (filter paper), CNC, CNC-COOH, and CNC-COO-CB12 are suspended or dissolved in DMSO-d_6 and analyzed by ^{1}H NMR spectroscopy at room temperature. Whatman filter paper, CNC, and CNC-COOH did not dissolve in DMSO-d_6 and no proton peaks apart from the protons in the solvent are observed in the spectra (Figure S1). The sample, CNC-COO-CB12, is soluble in DMSO-*d6* at 25 °C (Figure 2). The ester proton peak appears at 4.08 ppm, thus indicating the proof of functionalization. The resonance peaks of the a, b, c, and d hydrogen atoms from the CB12 moiety appear at 7.86, 7.83, 7.69, and 7.04 ppm, respectively. The resonance peaks at 4.01 and 3.97 ppm result from the ester and the ether groups, respectively. The signals at 3.58 and 3.36 ppm are assigned to the hydrogen atoms of the anhydro glucose unit of the cellulose nanocrystal. The signals from the upfield are assigned to the hydrogen atoms of the aliphatic chain attached to the CB12 moiety. These results agree with the previous reports.[23] The degree of substitution (DS, i.e., the number of CB12 chains grafted per anhydro glucose unit onto the surface of the CNCs) is determined by integrating the corresponding NMR peaks and using the following formula.

Degree of substitution = $(I_{7.04}/I_{4.01}) * 100$

$= (2/2.29) * 100$

$= 87.34\%$

Where I, is the integration value of the observed peaks. The high degree of substitution can be attributed to the high aspect ratio of the TEMPO-oxidized cellulose nanocrystals (CNC-COOH) and the presence of the twelve methylene spacer group attached to the cyanobiphenyl molecule attributed to the greater interactions between the CB12 and the CNCs.

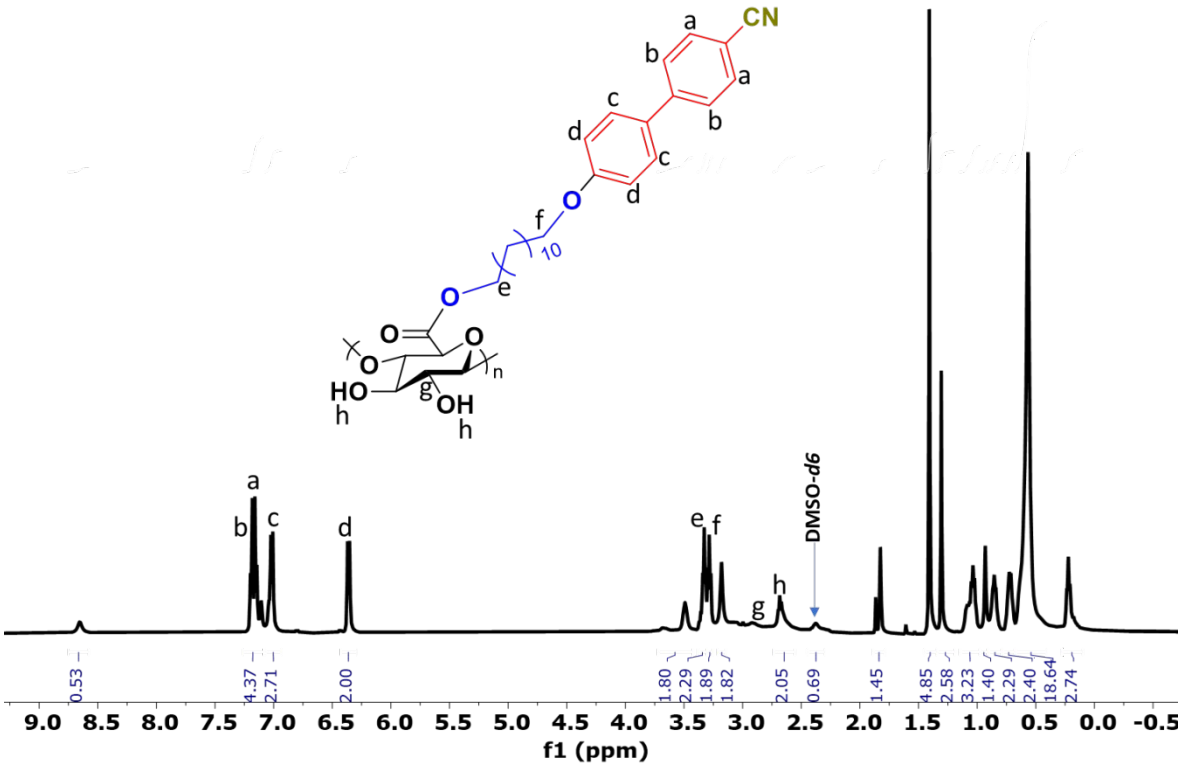

Figure 2: ^{1}H NMR for the CNC-COO-CB12 in DMSO-*d6* at room temperature.

Furthermore, solid-state cross-polarization magic angle spinning (CP-MAS) ^{13}C NMR studies show that neither crystallinity nor morphology of CNCs is affected by the surface modifications (Figure 3). The signal position of C6 at 66 ppm is a characteristic peak for cellulose I.[24] The shoulder signal around 64 ppm and the small broad signal around 84 ppm in CNC are known to arise from the C6 and C4 carbons in the amorphous region, respectively.[24] The sharp signal around 98 ppm in the spectrum of the CNC is assigned to the α-type anomeric Cl carbon of the reducing end glucose residue in the cellulose oligomers.[24] The appearance of carbonyl-C peaks at around 175 to 160 ppm CNC samples confirms that CNCs indeed oxidized into CNC-COOH.

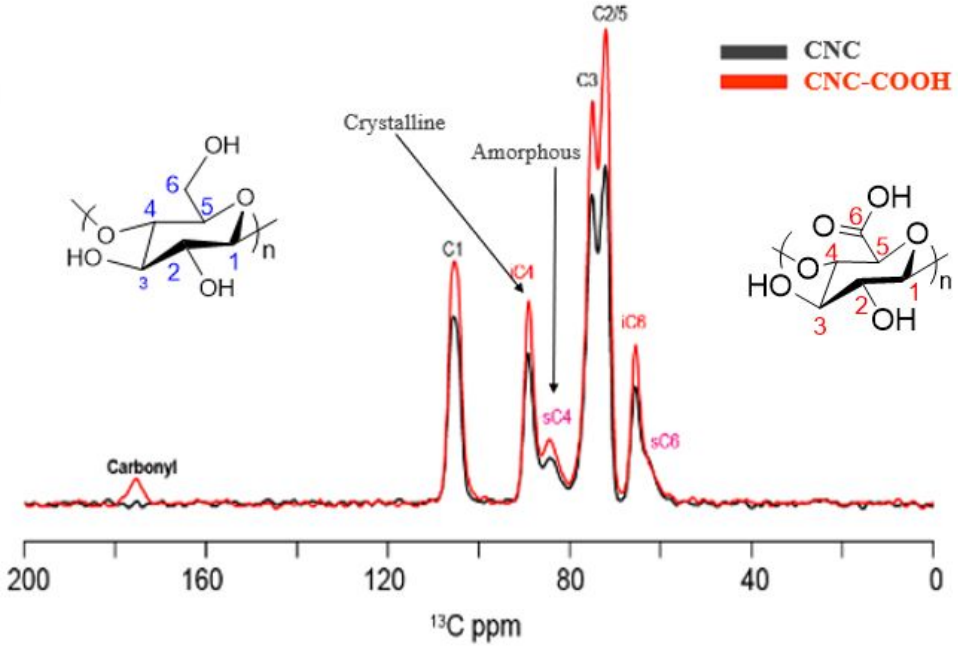

Figure 3: Solid-state cross-polarization ^{13}C-NMR spectra of CNC and CNC-COOH samples.

Further functionalization of CNC-COOH with CB12-OH results in CNC-COO-CB12 with aromatic carbon peaks between 140 to 130 ppm and aliphatic carbon signals at around 50 to 10 ppm (Figure S2). The area of the peak that corresponds to the C6 amorphous region, labeled as C6 (small shoulder on the right, Figure 3), is observed to decrease for the functionalized CNC products when compared to the untreated CNCs (Figure S4 and S5). This indicates the carboxylation and the resultant esterification of the C6 hydroxyl groups in the amorphous region.

The FTIR spectrum of the hydrolyzed cellulose nanocrystals (CNC) displays characteristic patterns corresponding to cellulose I (Figure S3). The peak at 1643 cm^{-1} could be formed due to the bending mode of adsorbed water.[25] The peak at 1445 cm^{-1} may be due to CH_2 bending vibration.[26] The sharp transmittance peak around 1388 cm^{-1} represents a bending of OH groups.[27] The peak at 1174 and 1120 cm^{-1} corresponds to C-O asymmetric bridge stretching.[27] The peak at 1057 cm^{-1} may be due to C-O-C pyranose ring skeletal vibration.[27] The CNC-COOH FTIR curve

is comparable with that of CNC with a nearly similar shape, except that it has some functional variations. For instance, the presence of a high-intensity peak at 1744 cm^{-1} is characteristic of the CNC-COOH spectrum, thus demonstrating the presence of the C=O group in the carboxylate group. Moreover, the CNC-COO-CB12 curve is slightly distinctive due to the presence of CN stretching at 2234 cm^{-1}, C-O stretching at 1255 and 1059 cm^{-1}, and benzene aromatic C=C unit at 1606 cm^{-1}, emanating from the CB12. These results demonstrate that the esterification process is successful.

Aspect Ratio of Cellulose Nanocrystals

The CNC and CNC-COOH aspect ratios are determined by TEM and the micrographs are presented in Figures 4 and Figure 5, respectively. The average length of the cellulose nanocrystals observed is ~200 nm, and the width is ~30 nm. The aspect ratio of the sample is 6 (±1.2).

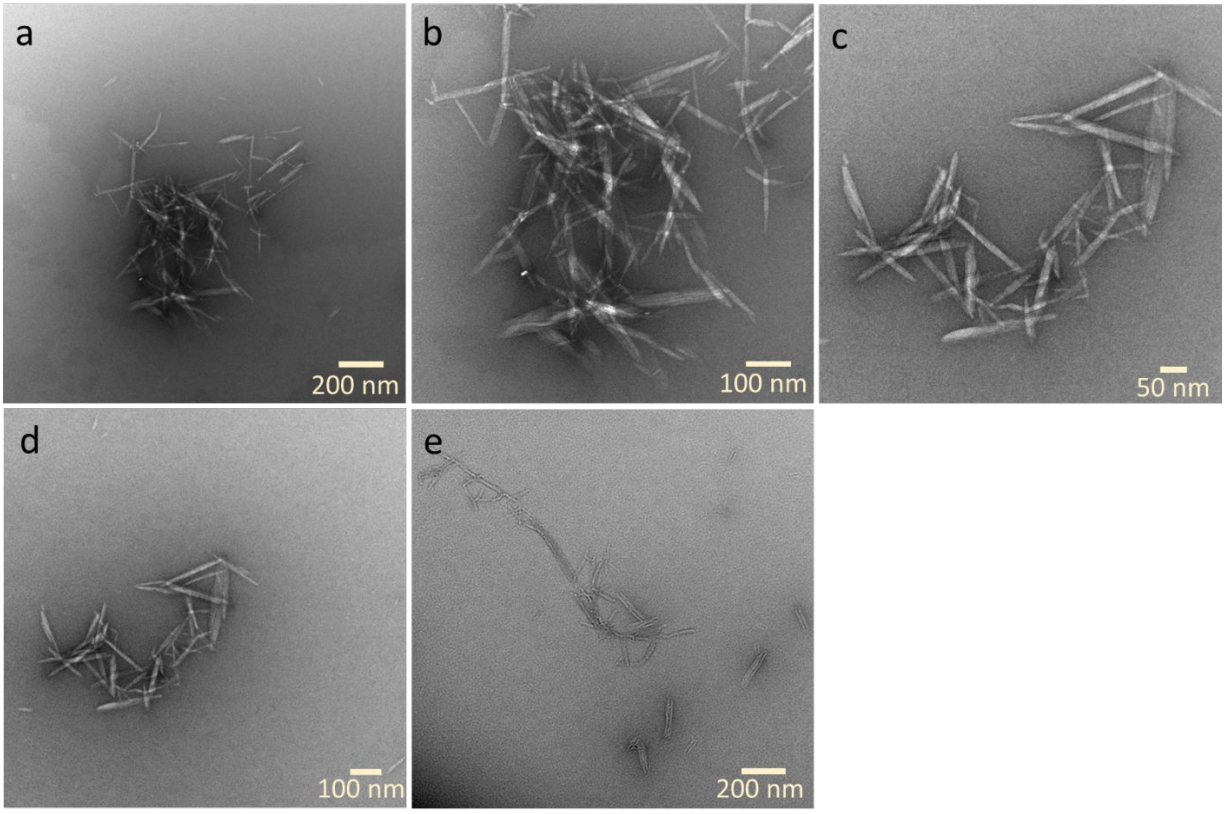

Figure 4: (a)-(e) TEM micrographs of CNCs nanocrystals at different magnifications. The nanocrystals are dispersed in water at a concentration of 0.5 mg/mL. The samples are negatively stained using a 0.5 wt.% of uranyl acetate before imaging.

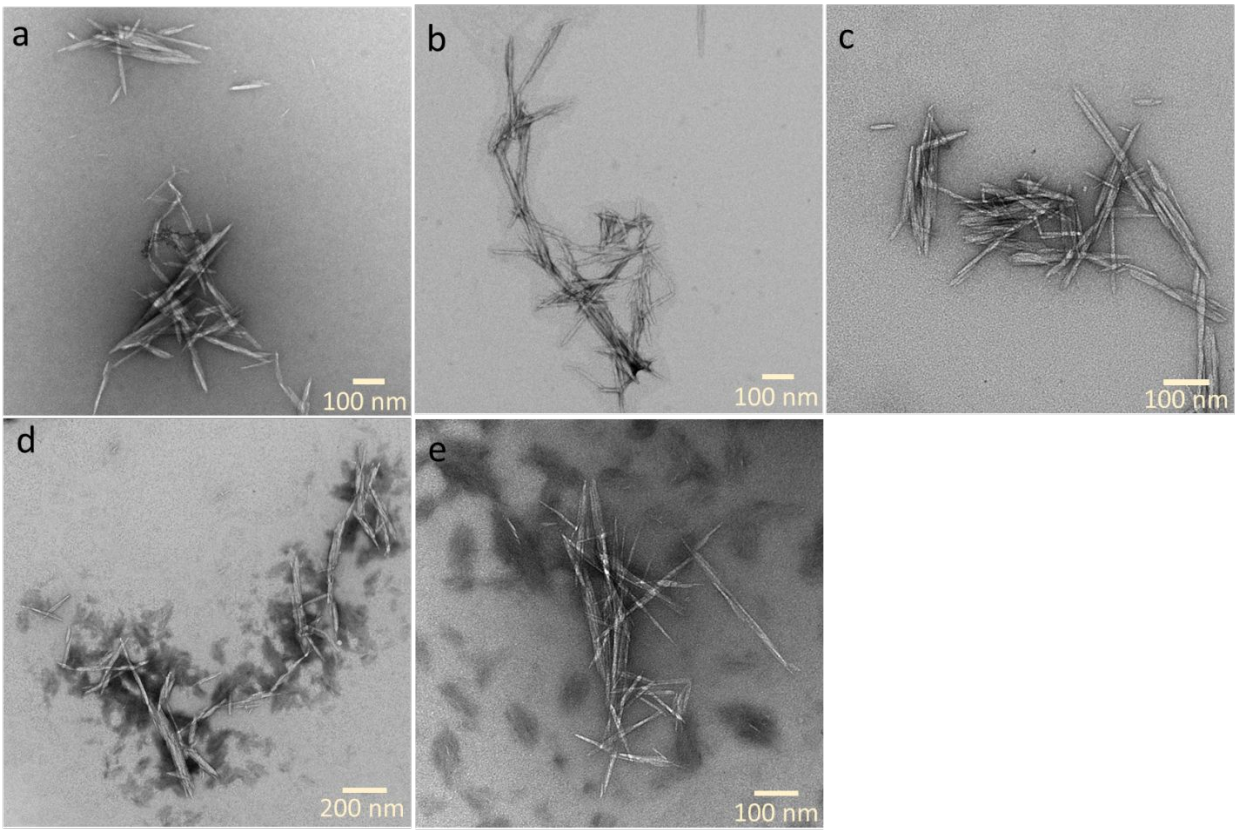

Figure 5: (a)-(e) TEM micrographs of CNC-COOH nanocrystals at different magnifications. These nanocrystals are dispersed in water at a concentration of 0.5 mg/mL. The sample is negatively stained using 0.5 wt.% of uranyl acetate before imaging.

Morphological Properties

The surface features of the CNC, CNC-COOH and CNC-COO-CB12 films prepared on carbon tape and sputter coated with a thin gold conductive layer are examined by SEM. The SEM images of CNC and CNC-COOH in Figures S7 and S8 (ESI) show collapsed helically twisted or cholesteric structures on the surface of dried films. The SEM images of CNCs and CNC-COOH are similar to those of cholesteric CNC, from distinct tactoids to long-range lamellar structures composed of helically twisted fibrils frozen within dried films.[28] In contrast, the SEM data of CNC-COO-CB12 (Figure S9) does not show any helical organization.

Thermal properties

The thermal degradation behavior of cellulose W.P., CNC, CNC-COOH, and CNC-COO-CB12 are investigated by thermogravimetric analyses (TGA, Figure 7). Cellulose W.P. reveals the onset of thermal degradation at around 350 °C.[29] In most cases, the onset degradation of CNCs occurs between 200 -300 °C, depending on the particle type and surface modification. The CNCs used in this study had an onset degradation temperature of 260 °C.[29] The chemical modification of CNCs to CNC-COOH and CNC-COO-CB12 altered their respective onset degradation temperatures. Weight loss curve of CNC-COO-CB12 ester differs remarkedly from the presented forms of cellulose W.P., CNC, and CNC-COOH with an early onset thermal degradation at around 125 °C, which could be due to moisture, and a major degradation occurred at around 325 °C. The CNC-COO-CB12 had the lowest onset degradation temperature of 220 °C. This lower onset degradation temperature in CNC-COO-CB12 could be due to a labile ester formation and subsequent decrease in hydrogen bonding between COOH and OH groups.[30, 31] Esterification improved the weight loss resistance of CNC-COO-CB12, which registers a higher total weight loss (TWL) and shorter 1% weight loss time (t1%) than CNC-COOH. The degradation temperature of TEMPO-oxidized cellulose crystals grafted with 4-((2-amnioethyl)amnio)-9-methyl-1,8-naphthalimide (TOCNC-AANI) reveals similar results on weight loss resistance ascribed to the covalent attachment of AANI.[32] Contrary results were obtained from the CNC tagged with cholesterol, whose weight loss resistance deteriorated compared to CNC. These results suggest that modified cellulose nanocrystals could undergo surface crosslinking after degradation of the modifying groups to enhance the in-carbonization of the cellulose nanocrystals.[33]

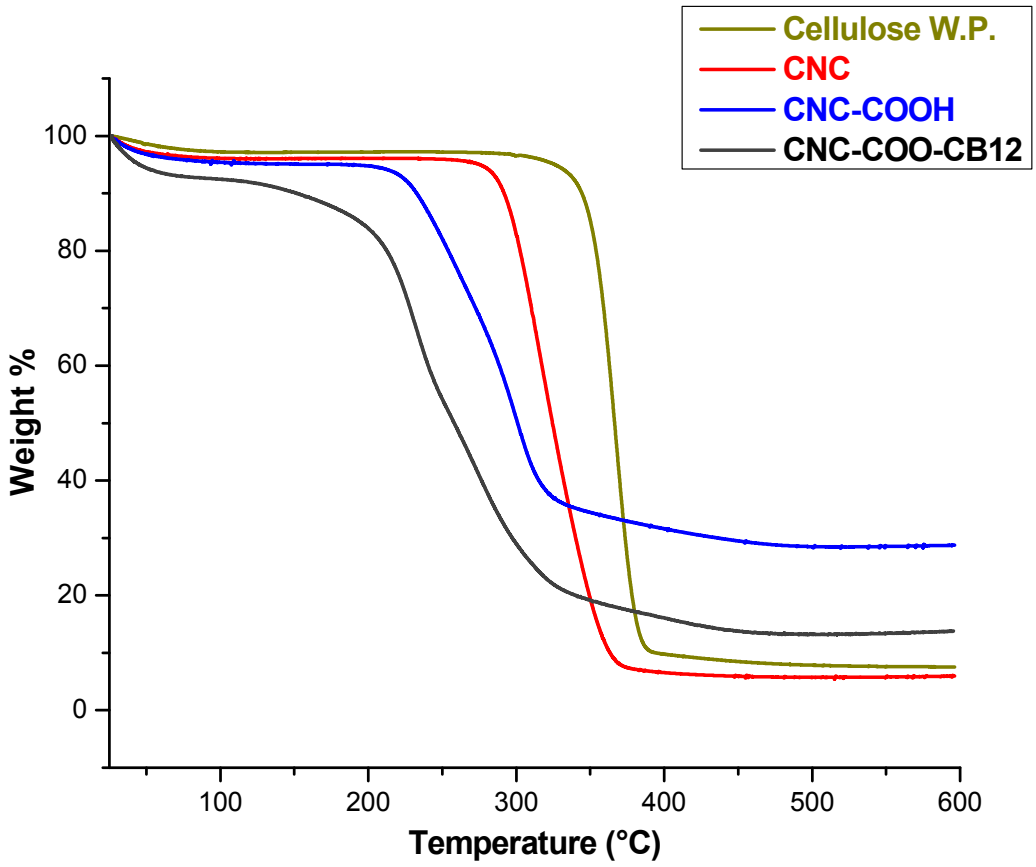

Figure 6: TGA traces showing thermal stability of Cellulose, W.P. CNC, CNC-COOH, and CNC-COO-CB12.

The thermal transitions of CNC-COO-CB12 are investigated using differential scanning calorimetry (DSC) and compared with CNC-COOH (Figure 7). Samples are first heated to 120 °C at a rate of 10 °C min^{-1} to remove the thermal history. Data from the subsequent first cooling and second heating cycles for CNC-COOH, CB12-OH, and, CNC-COO-CB12 are shown in Figure 7. CNC-COO-CB12 shows a glass transition temperature (T_g) at 10 °C and LC clearing transition (T_{LC}) at 43 °C accompanied by minor mesophase transitions at 35 °C and 30 °C, from the 1st cooling cycle. Similar transitions are observed on the second heating cycle, T_g at 40 °C and T_{LC}

at 74 °C, with a minor LC transition at 55 °C. Thermal transitions are mainly dependent on the CB12 side chain. In contrast to CNC-COO-CB12, CNC-COOH solid samples did not show any mesophase transition, while CB12-OH shows a mesophase transition around 60 °C and a melting transition at ~ 100 °C. We will elucidate the meso- and microstructure associated with the thermal transitions in CNC-COO-CB12 through temperature-controlled SAXS (T-SAXS) investigations.

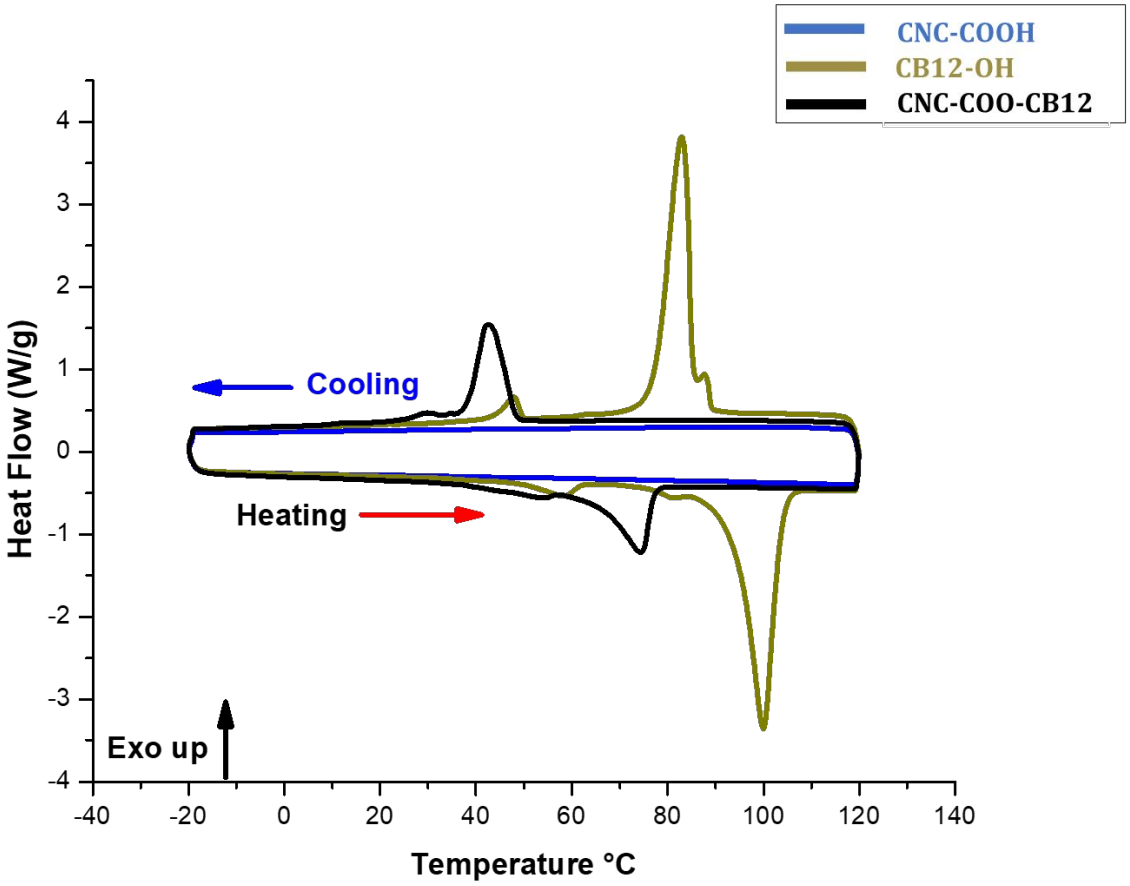

Figure 7: DSC overlay thermograms of heating and cooling cycles depicting the thermal transitions of CB12-OH, CNC-COOH, and CNC-COO-CB12 with a cooling rate of 10 °C min^{-1}. The cooling and heating transitions observed in CNC-COO-CB12 are reversible upon successive heat-cool cycles. These transitions are attributed to the CB12-OH moiety.

Microstructural and Crystallinity Analysis

The microstructure analysis of CNC-COO-CB12, CNC, CNC-COOH and CB12-OH are characterized by wide-angle X-ray scattering (WAXS) to study the effect of substitution and functionalization on the crystallinity of the CNC matrix (Figure 8). CNC exhibits four main diffraction peaks at 2θ = 14.6°, 16.4°, 20.3°, and 22.5°, attributed to the cellulose I_β crystalline structure (monoclinic unit cell, ICDD PDF 00-056-1718).[34] The estimated crystallinity index for CNC is 86.9%, and the crystallite size is 6.3 nm. The nearly invariant diffraction pattern of CNC-COOH (2θ = 14.7°, 16.5°, 20.4°, and 22.7°) compared to that of CNC suggests that the chemical modification has minimal impact on the local crystalline structure; the observed peak shift of ~0.1°(2θ) is probably due to the oxidation process. For both CNC and CNC-COOH, a diffraction peak representing the lateral packing of the cellulosic backbone (4.3 Å) is found at 2θ =20.3°. Covalently linking CB12-OH moieties to CNC-COOH results in a distinct change in the WAXS diffraction pattern. We focused on the diffraction peak in the lower angle range, where the first observable peak from CNC-COO-CB12 appears at (4.7°), corresponding to a length of 1.9 nm longer than that of CB12-OH (~ 1.64 nm), which presumably corresponds to the distance between the 12-methylene units spaced by the biphenyl groups after the head-to-tail π – π stacking. The increased length of CNC-COO-CB12, from 1.64 to 1.9 nm (Table inset in Figure 8), can be attributed to the larger distance between the cellulosic main chain backbones compared to that between the 12-methylene units. Several Braggs reflections are observed for CNC-COO-CB12, with some of them inheriting from those of CNC-COOH and others presumably related to the covalently linked CB12 and the lateral packing of the biphenyl core units (π-π stacking at 3.86 Å), which is not observed in CNC and CNC-COOH. Furthermore, CNC-COO-CB12 exhibit a

crystallinity index of 50.3% and crystallite size of 18.7 nm. The WAXS results of CNC-COO-CB12 indicate that partial crystallization of the bulk material is retained.

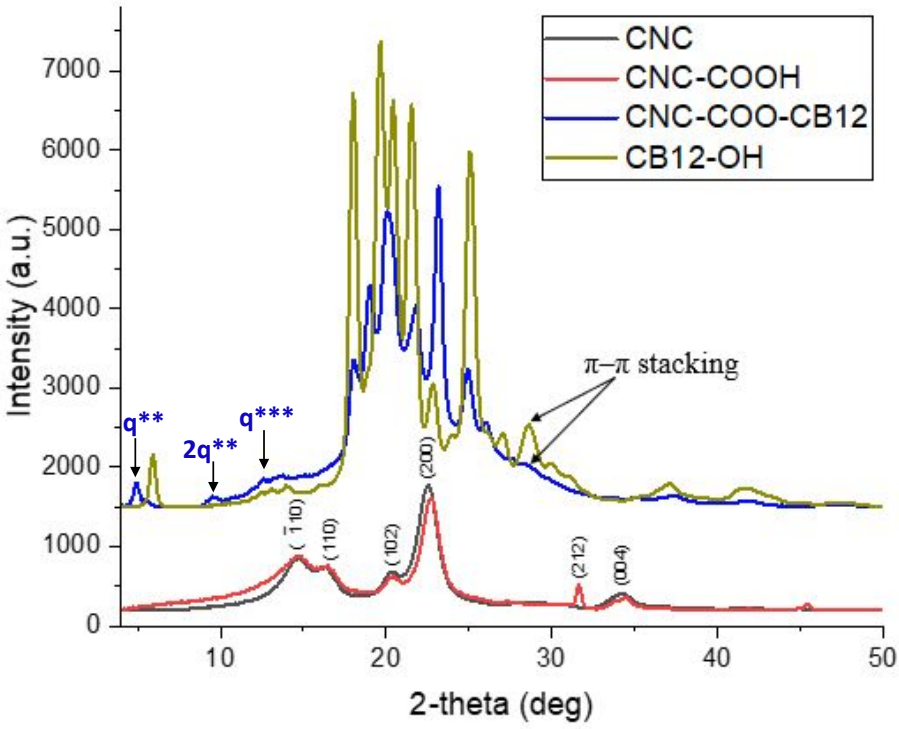

Parameters		
Sample	2 (degrees)	d spacing (nm)
CNC	14.85	0.6
	16.43	0.54
	20.63	0.43
	22.83	0.39
	34.8	0.26
CNC-COOH	14.93	0.59
	16.5	0.54
	20.63	0.43
	22.95	0.39
	34.73	0.26
CB12-OH	5.4	1.64
	12.83	0.69
	17.45	0.51
	18.89	0.47
	19.78	0.45
	20.81	0.43
	21.88	0.41
	24.61	0.36
	25.35	0.35
	28.47	0.31
CNC-COO-CB12	4.74	1.9
	12.46	0.71
	17.93	0.49
	19.88	0.45
	21.68	0.41
	22.88	0.39
	24.88	0.36
	28.88	0.31

Figure 8: 1D WAXS patterns overlay of **CNC**, **CNC-COOH**, **CB12-OH, and CNC-COO-CB12**. The CNC-COO-CB12 exhibits peaks that are attributed to both the CNC and CB12-OH. Here q**, 2q**, and q*** are Bragg reflections attributed to smectic mesophase, as is also observed in T-SAXS.

Presence of smectic polymorphism

To further investigate mesophase morphology in CNC-COO-CB12, both room temperature and temperature-controlled SAXS (T-SAXS) are employed (Figure 9). Multiple peaks from CB12 suggest that the materials form liquid crystalline smectic phases. The peak at q* is attributed to the diagonal spacing of the CNC backbone, assuming that the macromolecule self-assembles into a 3-

dimensional structure while maintaining the smectic ordering from the CB12 moiety. At room temperature, four Bragg reflections were initially observed at q^* (0.22 $Å^{-1}$, d_1 = 2.8 nm), q** (0.33 $Å^{-1}$, d_2 =1.9 nm), 2q** (0.65 $Å^{-1}$) and q_{***} (0.87 $Å^{-1}$, d_3 = 0.72 nm), respectively. The SAXS results seem to indicate interdigitated smectic formation, where the d_1, d_2, and d_3 could be attributed to smectic interdigitated formation (to be explained below). Such smectic phase disappears around 75 °C. The smectic polymorphism observed is common to thermotropic LC polymeric systems, where optimal decoupling between the backbone and LC mesogen is controlled by the type and length of spacer moiety.[22,35] There are at least two transition temperatures (T_{LC1} and T_{LC2}) along the thermal pathway from room T to high T and then back to room T [Figure 9(b)]. As $T_{LC2} > T > T_{LC1}$, the peak of q* disappears first, while the three peaks of q**, 2q** and q*** disappear simultaneously at $T > T_{LC2}$. This suggests that the origin of q** and q*** should come from the same structure. We also observed that the thermal response and structural transformation associated with cooling and heating processes are reversible (considering hysteresis). The hypothetical structural transformation is proposed in Figure 9(c). The high-T sample ($T > T_{LC2}$) demonstrates an isotropic state, whose SAXS shows monotonic decay with no liquid crystalline peak. The cooling process ($T_{LC2} > T > T_{LC1}$) promotes the neighboring CNC-COO-CB12 polymers to connect with each other through the $\pi - \pi$ stacking of the biphenyl on the CB12 side chains. Further cooling results in a more ordered square lattice structure (with a repeat unit composed of four chains) on the cross-sectional plane of the polymer bundles ($T < T_{LC1}$) based on SAXS and DSC data. We propose that the first transition takes place as the adjacent CNC polymers have a well-defined spacing of 1.9 nm ($d_2 = \frac{2\pi}{q^{**}}$) between the polymer backbones. As T continuously decreases below T_{LC1}, a new well-defined spacing of 2.8 nm ($d_1 = \frac{2\pi}{q^{*}}$) corresponding to the

diagonal distance of the square lattice. However, the square lattice structure takes long time to form in order to overcome the restricted motion of local polymer segments.

The peaks at q~0.4 Å^{-1} and ~0.8 Å^{-1} indicated by K* are from the Kapton background; these persist in different temperature values. The morphological evolutions are consistent with results obtained from DSC.

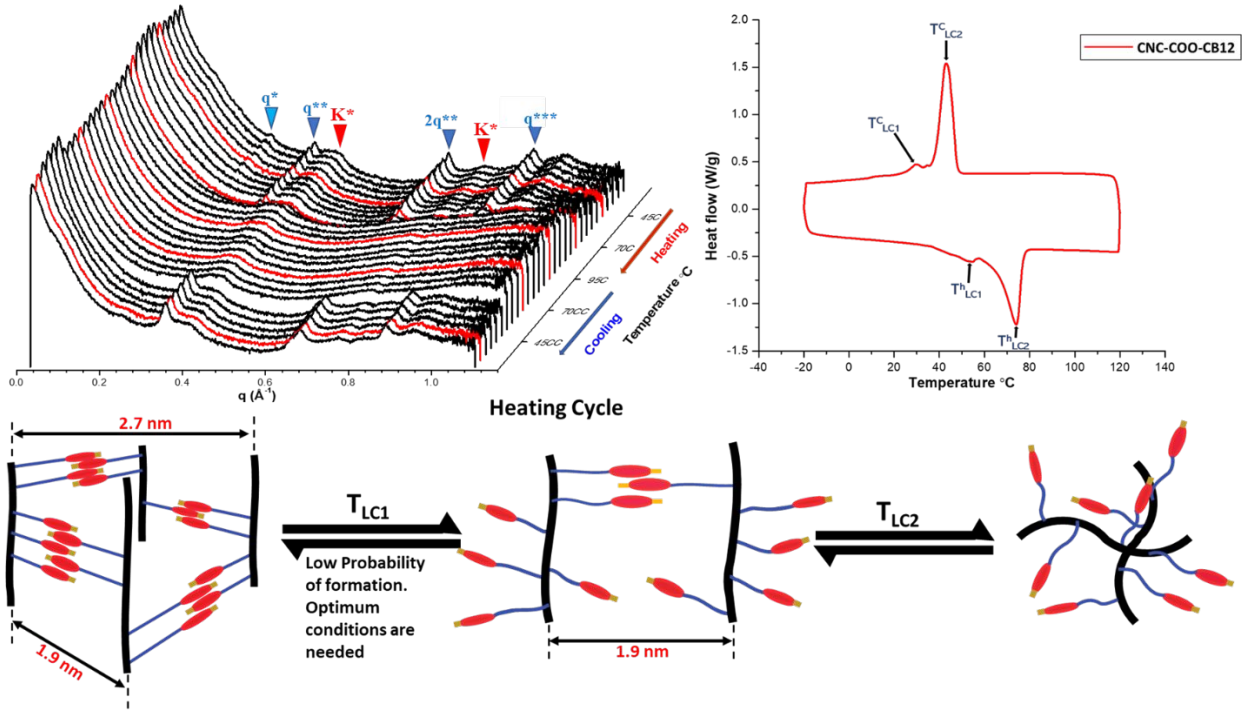

Figure 9: Meso-structural evolution of CNC-COO-CB12 from compression-molded film. (a) T-SAXS analysis. The CNC-COO-CB12 solid platform shows smectic polymorphism (q* (d_1), q** (d_2), 2q**, and q*** (d_3) between room temperature and 75 °C. (b) DSC analysis. (c) Schematic of the microstructural analysis that correlates with both T-SAXS and DSC.

Optical properties

The cholesteric nature of cellulose nanocrystals upon self-assembly is characterized by continuously twisted arrangements of helical pitches, which are impacted by dispersion composition, ionic strength of the medium, particle size, and temperature (Figure 10). At 3 w% of CNC, CNC-COOH, and CNC-COO-CB12 in LiCl/ DMAC solutions, both isotropic and anisotropic phases coexist due to the free mobility of the sample particles. However, the slow evaporation of DMAC increases the CNC, CNC-COOH, and CNC-COO-CB12 concentrations, thus limiting their mobility. The subsequent self-assembly results in thin films with characteristic liquid crystalline order. In Figure (10) image (a) shows the LiCl/DMAc film, (b) CNC film with the cholesteric ordering, (c) CNC-COOH film with the cholesteric ordering, and (d) CNC-COO-CB12 with a smectic ordering characterized by the loss of color compared to the preceding films. The presence of CB12 grafted onto the cellulose nanocrystals hinders chiral nematic interaction between the CNC rods but enhances interactions of the CB12 mesogens during self-assembly, thus leading to the disappearance of the iridescent colors. This, in turn, leads to the disappearance of chiral nematic or cholesteric liquid crystalline order and the appearance of smectic liquid crystalline order.

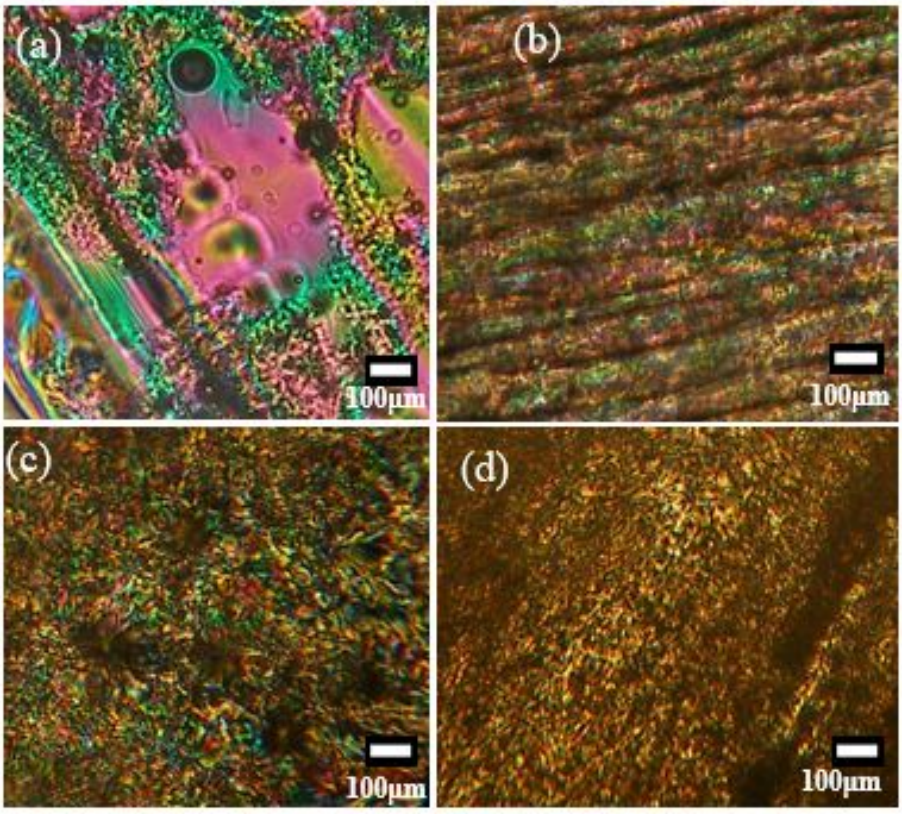

Figure 10: Films observed from POM **(a)** LiCl/DMAC, **(b)** 3wt% **CNC** in LiCl/DMAC, **(c)** 3wt% **CNC-COOH** in LiCl/DMAC **(d)** 3wt% **CNC-COO-CB12** in LiCl/DMAC.

For UV-Visible reflection measurements, the free-standing films (~ 0.3 mm in thickness) are prepared by solution casting technique on the polyimide Kapton films and annealed at a temperature of 50 ^{0}C, quenched to room temperature to kinetically trap the corresponding mesophases using cold air or liquid nitrogen to room temperature, thus allowing preservation of the mesophases. UV visible spectra (Figure 11) show that CNC and CNC-COOH have a broad reflection expected of unaligned cholesteric 1D photonic mesophase,[36] but CNC-COO-CB12 only shows CB12 reflection in the deep UV.[37] All the sample films measured by UV−visible spectroscopy at a normal incidence exhibited a high reflectivity in the visible light wavelength range. The presence of CB12 in the CNC-COO-CB12 samples significantly reduced the

transmittance of the films in this region. This could be attributed to the bulk nature of the CB12, which caused more scattering of the incident light, reducing the transparency of resulting films. The CNC-COO-CB12 spectrum shows a maximum transmission wavelength (λ_{max}) at 278.5 nm. The literature reported maximum transmission wavelength (λ_{max}) of pure CB12 is at 303.0 nm, which is attributed to the π- π* transition bands.[37, 38] The interaction of the cyanobiphenyl with the 12 methylene spacers and cellulose nanocrystals could have resulted in the alteration of the transmission wavelength of the cyanobiphenyl moiety with the blue shift.

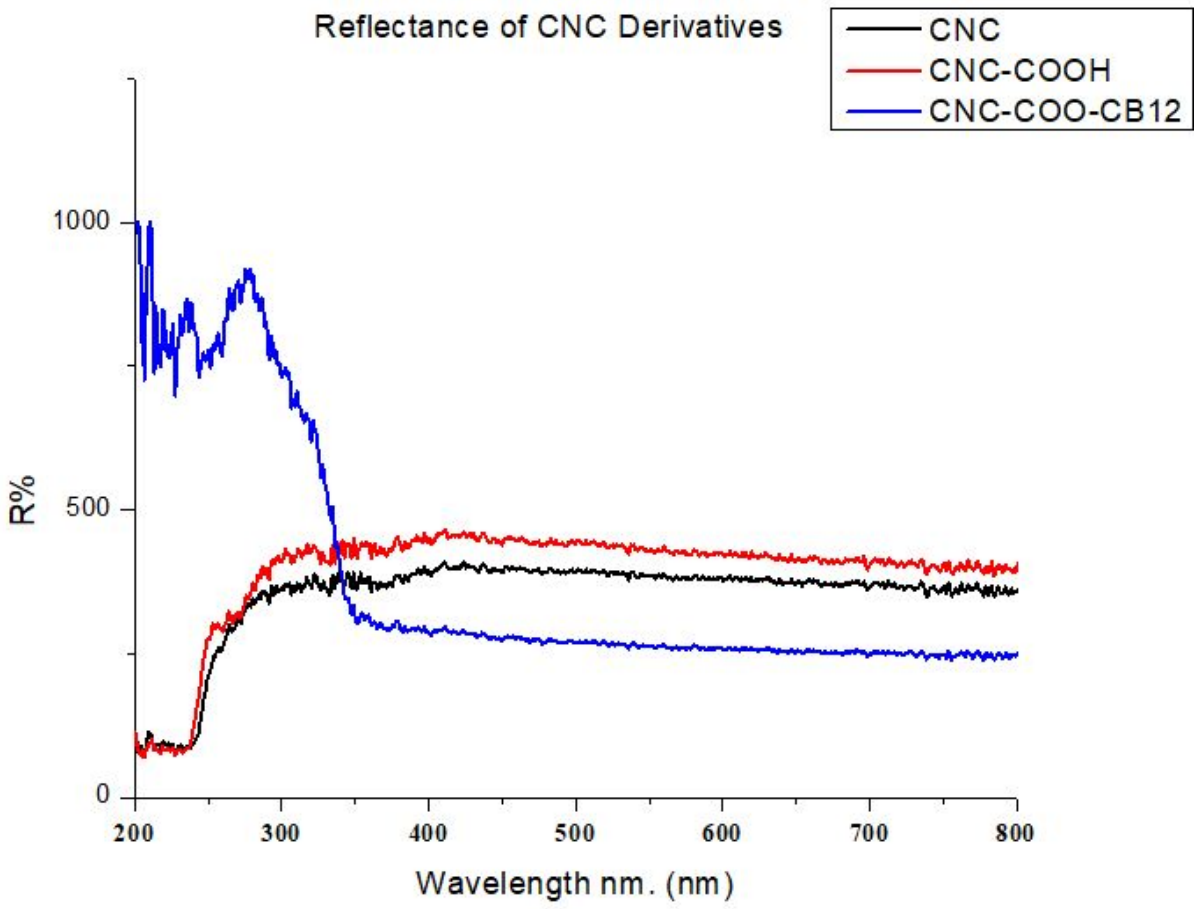

Figure. 11: Light reflection of CNC, CNC-COOH, and CNC-COO-CB12 film samples prepared by solution casting technique and annealing at 50 ˚C temperatures.

The data obtained from WAXS, POM, SEM, and SAXS reveal that both CNC and CNC-COOH undergo supramolecular self-assembly to form chiral nematic liquid crystalline phase. The introduction of a thermotropic liquid crystalline molecule (CB12) by covalent chemical conjugation onto the cellulosic matrix resulted in a solid platform that self-assembled into a smectic mesogenic phase without the application of an external field. This interplay of LC properties of CNCs and the thermotropic liquid crystals could be utilized for creating functional layered templates.

Conclusion

We report the molecular design, synthesis, and characterization of cellulose nanocrystals with a thermotropic liquid crystalline cyanobiphenyl with a 12-methylene spacer. This, to the authors' knowledge, is the first attempt to show the effect of the thermotropic liquid crystalline cyanobiphenyl with a 12-methyelene spacer. The impact of the thermotropic LC molecule on the hierarchical self-assembly, thermal, morphological, and optical properties of cellulose nanocrystals are investigated. The functionalization of CNC-COOH with cyanobiphenyl and improved dissolution of CNC-COO-CB12 is investigated by the ^{1}H NMR spectroscopy and revealed a functionalization efficiency of 87.34%. FTIR spectroscopy of the solid-state platform further reveals the functionalization of the CNCOOH by the characteristic C≡N stretching peak from the cyanobiphenyl. The coexistence of thermotropic π-π interaction and LC-LC interactions predominate the CNC-CNC interactions, thus leading to smectic polymorphism at room temperature. This smectic mesophase behavior of CNC-COO-CB12 upon self-assembly is the first one to be reported. The presence of π–π thermotropic interactions coexisting with chiral nematic from the CNCs manifests as visible reflections from π–π* transitions in the visible spectrum. In this work, we show that using supramolecular π–π interactions of the thermotropic liquid

crystalline molecule with a 12-methylene spacer, changes the self-assembly of CNC from chiral nematic to smectic ordering. This new platform, CNC-COO-CB12, can be further aligned and ordered by directed self-assembly methods producing highly ordered, degradable templates from sustainable sources.

Acknowledgment:

This work is supported by the National Science Foundation under DMR-1507045. The central instrumentation facilities at the Institute of Materials Science and Chemistry Department at UConn are acknowledged. The acquisition of the SAXS instrument was partially supported through an NSF grant (MRI-1228817). The authors thank Prof. Steven Suib and his research group for help with UV–visible measurements. The authors thank the Institute of Materials Science, Center for Advanced Microscopy, Materials Analysis (CAMMA) and Dr. Roger Ristau, Dr. Lichun Zhang and Dr. Haiyan Tan at CAMMA for technical support on Teneo LVSEM instrument.

Conflict of Interest: The authors declare no conflict of interest.

References

1. Prasanna, N. S.; Mitra, J., Isolation and characterization of cellulose nanocrystals from Cucumis sativus peels. *Carbohydrate Polymers* **2020,** *247*, 116706.
2. Melikoğlu, A. Y.; Bilek, S. E.; Cesur, S., Optimum alkaline treatment parameters for the extraction of cellulose and production of cellulose nanocrystals from apple pomace. *Carbohydrate polymers* **2019,** *215*, 330-337.
3. Yu, H.; Qin, Z.; Liang, B.; Liu, N.; Zhou, Z.; Chen, L., Facile extraction of thermally stable cellulose nanocrystals with a high yield of 93% through hydrochloric acid hydrolysis under hydrothermal conditions. *Journal of Materials Chemistry A* **2013,** *1*, 3938-3944.
4. Hegmann, T.; Gonçalves, D., Chirality Transfer from an Innately Chiral Nanocrystal Core to a Nematic Liquid Crystal: Surface-Modified Cellulose Nanocrystals. *Angewandte Chemie (International ed. in English)* **2021,** *60*, 17344.
5. Upton, B. M.; Kasko, A. M., Strategies for the conversion of lignin to high-value polymeric materials: review and perspective. *Chemical Reviews* **2016,** *116*, 2275-2306.

6. Wu, Z.-Y.; Liang, H.-W.; Chen, L.-F.; Hu, B.-C.; Yu, S.-H., Bacterial cellulose: a robust platform for design of three dimensional carbon-based functional nanomaterials. *Accounts of Chemical Research* **2016,** *49*, 96-105.
7. Giese, M.; Spengler, M., Cellulose nanocrystals in nanoarchitectonics–towards photonic functional materials. *Molecular Systems Design & Engineering* **2019,** *4*, 29-48.
8. Lagerwall, J. P.; Schütz, C.; Salajkova, M.; Noh, J.; Hyun Park, J.; Scalia, G.; Bergström, L., Cellulose nanocrystal-based materials: from liquid crystal self-assembly and glass formation to multifunctional thin films. *NPG Asia Materials* **2014,** *6* (1), e80-e80.
9. Marchessault, R.; Morehead, F.; Walter, N., Liquid crystal systems from fibrillar polysaccharides. *Nature* **1959,** *184*, 632-633.
10. Revol, J.-F.; Bradford, H.; Giasson, J.; Marchessault, R.; Gray, D., Helicoidal self-ordering of cellulose microfibrils in aqueous suspension. *Internaltional Journal of Biological Macromolecules* **1992,** *14* (3), 170-172.
11. George, J.; Sabapathi, S. N., Cellulose nanocrystals: synthesis, functional properties, and applications. Nanotechnology, Science and Applications 2015, 8, 45-54.
12. Dumanli, A. G. m.; Van Der Kooij, H. M.; Kamita, G.; Reisner, E.; Baumberg, J. J.; Steiner, U.; Vignolini, S., Digital color in cellulose nanocrystal films. *ACS applied materials & interfaces* **2014,** *6*, 12302-12306.
13. Xu, M.; Li, W.; Ma, C.; Yu, H.; Wu, Y.; Wang, Y.; Chen, Z.; Li, J.; Liu, S., Multifunctional chiral nematic cellulose nanocrystals/glycerol structural colored nanocomposites for intelligent responsive films, photonic inks and iridescent coatings. *Journal of Materials Chemistry C* **2018,** *6*, 5391-5400.
14. Kelly, J. A.; Shukaliak, A. M.; Cheung, C. C.; Shopsowitz, K. E.; Hamad, W. Y.; MacLachlan, M. J., Responsive photonic hydrogels based on nanocrystalline cellulose. *Angewandte Chemie International Edition* **2013,** *52*, 8912-8916.
15. Vollick, B.; Kuo, P.-Y.; Therien-Aubin, H.; Yan, N.; Kumacheva, E., Composite cholesteric nanocellulose films with enhanced mechanical properties. *Chemistry of Materials* **2017,** *29*, 789-795.
16. Xu, Q.; Yi, J.; Zhang, X.; Zhang, H., A novel amphotropic polymer based on cellulose nanocrystals grafted with azo polymers. *European Polymer Journal* **2008,** *44*, 2830-2837.
17. Delepierre, G.; Heise, K.; Malinen, K.; Koso, T.; Pitkänen, L.; Cranston, E. D.; Kilpeläinen, I.; Kostiainen, M. A.; Kontturi, E.; Weder, C., Challenges in synthesis and analysis of asymmetrically grafted cellulose nanocrystals via atom transfer radical polymerization. *Biomacromolecules* **2021,** *22*, 2702-2717.
18. Dong, Y. M.; Zhao, Y. Q.; Zeng, E. M.; Yang, L. L.; Ge, Q.; Hu, X. L. In *A Dendronized Cellulose Derivative and Its Thermotropic Liquid Crystal and Lyotropic Cholesteric Liquid Crystal Behaviors*, Advanced Materials Research, Trans Tech Publ: 2011; pp 2620-2623.
19. Hu, T.; Xie, H.; Xiao, J.; Zhang, H.; Chen, E., Design, synthesis, and characterization of a combined main-chain/side-chain liquid-crystalline polymer based on ethyl cellulose. *Cellulose* **2010,** *17*, 547-558.
20. Chang, C.; Duan, B.; Cai, J.; Zhang, L., Superabsorbent hydrogels based on cellulose for smart swelling and controllable delivery. *European polymer journal* **2010,** *46*, 92-100.
21. Liu, S.; Low, Z. X.; Xie, Z.; Wang, H., TEMPO-oxidized cellulose nanofibers: A renewable nanomaterial for environmental and energy applications. *Advanced Materials Technologies* **2021,** *6*, 2001180.

22. Deshmukh, P.; Gopinadhan, M.; Choo, Y.; Ahn, S.-k.; Majewski, P. W.; Yoon, S. Y.; Bakajin, O.; Elimelech, M.; Osuji, C. O.; Kasi, R. M., Molecular design of liquid crystalline brush-like block copolymers for magnetic field directed self-assembly: A platform for functional materials. *ACS Macro Letters* **2014,** *3*, 462-466.
23. Abu Hasan Howlader, M., Preparation, functionalization and derivation of nanocrystalline cellulose. **2015**: http://lib.buet.ac.bd:8080/xmlui/handle/123456789/3116

24. Isogai, A.; Usuda, M.; Kato, T.; Uryu, T.; Atalla, R. H., Solid-state CP/MAS carbon-13 NMR study of cellulose polymorphs. *Macromolecules* **1989,** *22*, 3168-3172.
25. Hinterstoisser, B.; Salmén, L., Application of dynamic 2D FTIR to cellulose. *Vibrational Spectroscopy* **2000,** *22*, 111-118.
26. He, Q.; Wang, Q.; Zhou, H.; Ren, D.; He, Y.; Cong, H.; Wu, L., Highly crystalline cellulose from brown seaweed Saccharina japonica: isolation, characterization and microcrystallization. *Cellulose* **2018,** *25*, 5523-5533.
27. Sun, X.-F.; Sun, R.-C.; Su, Y.; Sun, J.-X., Comparative study of crude and purified cellulose from wheat straw. *Journal of agricultural and food chemistry* **2004,** *52*, 839-847.
28. Wang, P.-X.; Hamad, W. Y.; MacLachlan, M. J., Structure and transformation of tactoids in cellulose nanocrystal suspensions. *Nature communications* **2016,** *7*, 1-8.
29. Habibi, Y., Key advances in the chemical modification of nanocelluloses. *Chemical Society Reviews* **2014,** *43*, 1519-1542.
30. Salam, A.; Lucia, L. A.; Jameel, H., Fluorine-based surface decorated cellulose nanocrystals as potential hydrophobic and oleophobic materials. *Cellulose* **2015,** *22*, 397-406.
31. Pourmoazzen, Z.; Sadeghifar, H.; Chen, J.; Yang, G.; Zhang, K.; Lucia, L., The morphology, self-assembly, and host-guest properties of cellulose nanocrystals surface grafted with cholesterol. *Carbohydrate Polymers* **2020,** *233*, 115840.
32. Wu, W.; Song, R.; Xu, Z.; Jing, Y.; Dai, H.; Fang, G., Fluorescent cellulose nanocrystals with responsiveness to solvent polarity and ionic strength. *Sensors and Actuators B: Chemical* **2018,** *275*, 490-498.
33. Shi, R.; Zhang, Z.; Liu, Q.; Han, Y.; Zhang, L.; Chen, D.; Tian, W., Characterization of citric acid/glycerol co-plasticized thermoplastic starch prepared by melt blending. *Carbohydrate Polymers* **2007,** *69*, 748-755.
34. Elazzouzi-Hafraoui, S.; Nishiyama, Y.; Putaux, J.-L.; Heux, L.; Dubreuil, F.; Rochas, C., The shape and size distribution of crystalline nanoparticles prepared by acid hydrolysis of native cellulose. *Biomacromolecules* **2008,** *9*, 57-65.
35. Bosire, R.; Ndaya, D.; Kasi, R. M., Cholesteric mesophase based 1D photonic materials from self-assembly of liquid crystalline block and random terpolymers containing chromonic molecules. *RSC Advances* **2021,** *11*, 14615-14623.
36. De La Cruz, J. A.; Liu, Q.; Senyuk, B.; Frazier, A. W.; Peddireddy, K.; Smalyukh, I. I., Cellulose-based reflective liquid crystal films as optical filters and solar gain regulators. *ACS Photonics* **2018,** *5* , 2468-2477.
37. Wu, S. T., A semiempirical model for liquid-crystal refractive index dispersions. *Journal of applied physics* **1991,** *69*, 2080-2087.
38. Verma, R.; Mishra, M.; Dhar, R.; Dabrowski, R., Single walled carbon nanotubes persuaded optimization of the display parameters of a room temperature liquid crystal 4-pentyl-4′ cyanobiphenyl. *Journal of Molecular Liquids* **2016,** *221*, 190-196.